American Mineralogist, Volume 87, pages 1291–1296, 2002

Hard-mode infrared spectroscopy of perovskites across the $CaTiO_3$-$SrTiO_3$ solid solution

HINRICH-WILHELM MEYER,[1,*] MICHAEL A. CARPENTER,[1] ANA I. BECERRO,[2] AND FRITZ SEIFERT[2]

[1] Department of Earth Sciences, University of Cambridge, Downing Street, Cambridge CB2 3EQ, U.K.
[2] Bayerisches Geoinstitut, Universität Bayreuth, D-95440 Bayreuth, Germany

ABSTRACT

Powder infrared spectra of perovskites across the $CaTiO_3$-$SrTiO_3$ solid solution have been collected at room temperature for the range 20–700 cm^{-1}. Frequency, intensity, and line broadening parameters vary with a pattern that appears to follow the development of the orthorhombic shear strain for the *Pnma* structure. The data are at least consistent with the $Pm3m \leftrightarrow I4/mcm$ transition at Sr-rich compositions being continuous in character and the tetragonal ↔ orthorhombic transition at ~62% $SrTiO_3$ content being discontinuous. In spite of the fact that crystals with intermediate composition have recently been shown to have *Pnma* rather than *Cmcm* symmetry, autocorrelation analysis of their IR spectra shows that they have features which distinguish them from crystals with *Pnma* symmetry for $CaTiO_3$ rich compositions. In particular, crystals of intermediate composition have the highest values of the line broadening parameter, Δcorr, for the solid solution, suggesting that they are characterized by relatively high degrees of local structural heterogeneity.

INTRODUCTION

Interest in members of the $CaTiO_3$-$SrTiO_3$ solid solution arises from its ferro- and dielectric properties (Lemanov 1997; Dec and Kleemann 1998; Kleemann et al. 1998) and from the possibility of using this system to form ceramics in which to immobilize radioactive waste elements (Ringwood 1985). Although it is known that $CaTiO_3$ and $SrTiO_3$ form a complete solid solution (Ceh et al. 1987), the sequence of phases across the solid solution at room temperature has recently been the subject of some debate (Hirata et al. 1996; Ball et al. 1998; Qin et al. 2000; Ranjan and Pandey 2001). For some time it has been known that at room temperature the $CaTiO_3$ end-member is orthorhombic with space group *Pnma*, while $SrTiO_3$ is cubic with space group *Pm*3*m*. Several authors reported the existence of a tetragonal phase with symmetry *I*4/*mcm* for X_{Sr} between 0.65 and 0.9 (Mitsui and Westphal 1961; Ball et al. 1998; Qin et al. 2000). Ball et al. (1998) concluded from X-ray powder diffraction experiments that an additional orthorhombic phase is present in the range 42–62% $SrTiO_3$, between the tetragonal phase and the orthorhombic Ca end-member phase, to which they assigned the space group *Cmcm*. Data from the literature for the location of transitions between these structures as a function of temperature and composition are summarized in Figure 1 (after Carpenter et al. 2001). However, Howard et al. (2001) and Ranjan et al. (2001) have shown by electron diffraction that the space group of thin plates of crystals with intermediate composition is *Pnma*, rather than *Cmcm*. The objectives of the present study were to investigate the structural evolution on a microscopic length scale and to characterize further the unusual behavior around the 1:1 composition of the solid solution.

Macroscopic strains due to phase transitions in the $CaTiO_3$-$SrTiO_3$ system have been analyzed recently by Carpenter et al. (2001), and the results for room temperature are shown in Figure 2. They are reproduced here to permit comparison with microscopic strain behavior interpreted from the new spectroscopic measurements. Lattice parameter variations of the reduced cubic unit cell across the solid solution (data from Qin et al. 2000) are shown in Figure 2a. The lattice parameter a_0 for a cubic reference state is shown as a solid line and is given by:

$$a_0 = 3.9052 - 0.0005803 \cdot X_{Ca} - 0.000001916 \cdot X_{Ca}^2 \quad (1)$$

where X_{Ca} represents the $CaTiO_3$ content in mol%. Symmetry-adapted strains were calculated according to:

$$e_1 = e_2 = \frac{\frac{a}{\sqrt{2}} - a_0}{a_0}, e_3 = \frac{\frac{c}{2} - a_0}{a_0} \quad (2)$$

for the tetragonal structure and according to:

$$e_1 = \frac{\frac{b}{2} - a_0}{a_0}, e_2 + e_3 = \frac{\frac{a}{\sqrt{2}} - a_0}{a_0} + \frac{\frac{c}{\sqrt{2}} - a_0}{a_0} \quad (3)$$

for the *Pnma* structure. The strains e_4, e_{tz}, e_{tx}, and e_a are defined as follows:

* Present address: Institut für Mineralogie, Universität Münster, Corrensstrasse 24, D-48149 Münster, Germany. E-mail: hwmeyer@nwz.uni-muenster.de

0003-004X/02/0010–1291$05.00

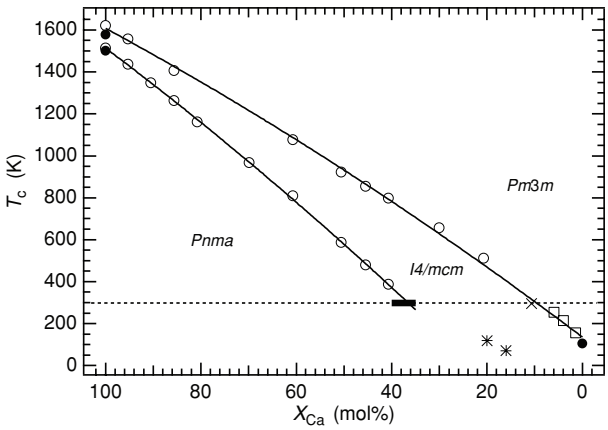

FIGURE 1. Phase diagram of the $Ca_xSr_{1-x}TiO_3$ binary system (taken from Carpenter et al. 2001). Different symbols mark the positions of phase transitions identified in the solid solution (see Carpenter et al. 2001 for full details). The samples analyzed in this study lie along the horizontal dashed line at room temperature.

$$|e_4| = \left| \frac{\frac{a}{\sqrt{2}} - a_0}{a_0} - \frac{\frac{c}{\sqrt{2}} - a_0}{a_0} \right| \tag{4}$$

and

$$e_{tz} = \frac{1}{\sqrt{3}}(2e_3 - e_1 - e_2) \tag{5}$$

$$e_{tx} = \frac{1}{\sqrt{3}}(2e_1 - e_2 - e_3) \tag{6}$$

$$e_a = (e_1 + e_2 + e_3). \tag{7}$$

Here, e_{tx} and e_4 are tetragonal and orthorhombic shear strains (respectively) for the *Pnma* structure and e_{tz} is the tetragonal shear strain for the *I*4/*mcm* structure. The volume strain e_a refers to both structures. The shear strain e_{tz} (Fig. 3) is continuous across the *Pm*3*m* ↔ *I*4/*mcm* transition, with a maximum of ~0.5%, which is about half the value of maximum e_4 for the Ca end-member composition. As for the intermediate structures in the solid solution, it is noticeable that they display very small e_4 and e_{tz} values, on the order of only ~0.1%, which indicates very small deviations from cubic geometry. The transition from the intermediate structures to the *I*4/*mcm* structure is marked by a clear discontinuity. The maximum value for e_4, the largest strain, is ~1.2% for the pure Ca end-member.

Hard mode infrared spectroscopy provides an effective method for characterizing the nature and mechanisms of structural phase transitions at a local (unit cell) length scale in crystalline materials (Bismayer 1990; Salje and Bismayer 1997). Until recently it might not have been the method of choice for perovskites. This is because powder absorption IR spectra for most perovskites contain broad overlapping peaks due to LO-TO splitting, which is a characteristic feature of strongly ionic compounds. The development of autocorrelation analysis, however, (Salje et al. 2000) means that it is now possible to extract quantitative line broadening information from such spectra.

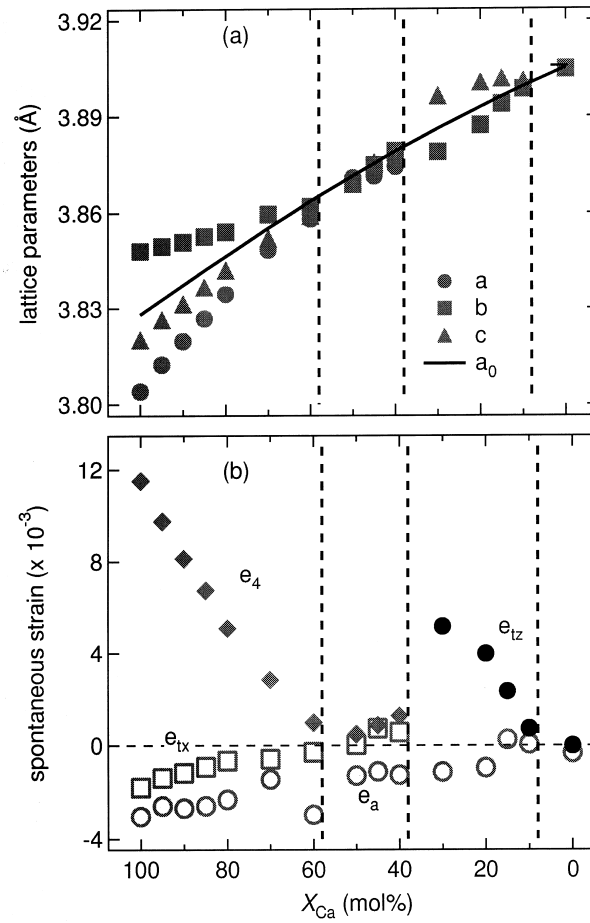

FIGURE 2. Strain behavior at room temperature across the $CaTiO_3$-$SrTiO_3$ solid solution (after Carpenter et al. 2001). Vertical broken lines show the locations of phase transitions taken from Figure 1. (**a**) Variation of lattice parameters of the reduced cubic unit cell. The solid curve shows the variation of the reference lattice parameter a_0, of the cubic structure used to calculate spontaneous strains. (**b**) Variation of shear strains with respect to a cubic parent structure. Filled circles represent the tetragonal shear strain of the *I*4/*mcm* structure and filled diamonds the orthorhombic shear strain of the *Pnma* structure. Note that these are significantly greater than the volume strain, e_a (open circles) in both structures and the tetragonal shear e_{tx} of the *Pnma* structure. The intermediate structure is characterized by having no significant shear strain.

EXPERIMENTAL METHOD

Powder samples in the system $CaTiO_3$-$SrTiO_3$ were synthesized from mixtures of $CaCO_3$, $SrCO_3$, and TiO_2, following the method of Qin et al. (2000) for the following compositions: X_{Sr} = 0.0, 0.05, 0.1, 0.15, 0.2, 0.3, 0.4, 0.5, 0.55, 0.6, 0.7, 0.8, 0.85, 0.9, and 1.0, where X_{Sr} is the mole fraction of $SrTiO_3$ compo-

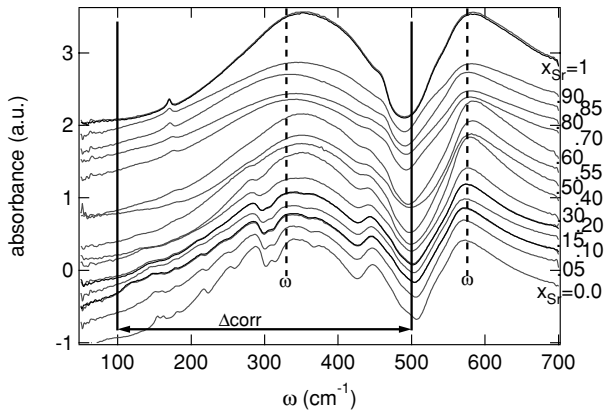

FIGURE 3. IR powder absorption spectra of $CaTiO_3$-$SrTiO_3$ samples. Continuous vertical lines indicate the spectral range chosen for the autocorrelation analysis, dashed vertical lines at ~330 and ~576 cm^{-1} show the peak regions where peaks were sought. Spectra for X_{Sr} = 0.10, 0.20, and 1.0 appear as heavier dark lines, because the spectra for two separate pellets prepared from these samples overlap, confirming the reproducibility of the spectroscopic method.

nent in the solid solution. To prepare IR pellets, the samples were ground by hand for 30 minutes in an agate mortar and were then mixed with enough polyethylene to attain a sample to dilutant ratio of 1:70 and a pellet weight of 100 mg. Pellets were pressed under vacuum and great care was taken to ensure that the grinding, mixing, and pressing sequence was reproducible. A pellet of pure polyethylene was prepared following the same conditions and was used as a reference. Data were collected in the FIR region between 20 and 700 cm^{-1} under vacuum at room temperature using a Bruker FIS 66v FT-IR spectrometer. The instrument resolution was set to 4 cm^{-1}. Spectra were calculated by Fourier transform of 1000 scans and recorded as absorbance $\alpha = -\log(I_{sample}/I_{reference})$, where I is the single beam transmission intensity.

RESULTS

In Figure 3 IR absorption spectra recorded at room temperature are shown for compositions $Sr_xCa_{1-x}TiO_3$. The $SrTiO_3$ (ST) end-member is shown at the top of the figure, followed by spectra of samples with increasing Ca content toward the pure Ca end-member (CT) at the bottom of the figure. The spectra are in generally good agreement with those reported by Hirata et al. (1996). Symmetry analysis indicates that fifteen normal modes are allowed in the cubic ST structure, three of which are acoustic and three more of which are silent. The remaining nine modes are three sets of triply degenerate IR active modes, which, due to long-range coulomb interactions, split into longitudinal and transversal modes (Fleury and Worlock 1968). These contribute to the very broad features centered around 330 and 580 cm^{-1}, respectively, which dominate all spectra across the solid solution. By increasing the Ca content the symmetry is reduced and the number of modes increased, so that in the orthorhombic CT phase, 25 IR active modes are possible (Lu and Hofmeister 1994). With increasing Ca content (moving downward on the graph) additional peaks appear (for example ~280 cm^{-1}) or vanish (170 cm^{-1}).

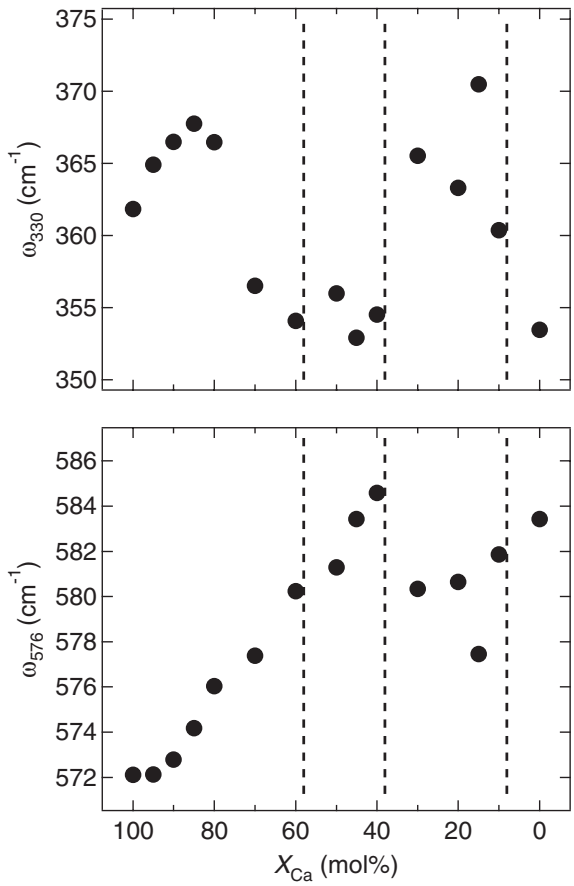

FIGURE 4. ω for the peaks at ~330 cm^{-1} and at ~576 cm^{-1}. Vertical lines, as in Figure 2, show the expected location of phase transitions. Although there is perhaps some correlation between frequency and transition behavior, the scatter in the data is too great to permit any confident interpretation at this stage.

Changes in wavenumber

Peak positions were obtained from smoothed first and second derivatives of the spectra using the commercial software package IGOR Pro (Wavemetrics, Inc., Oregon, U.S.A.). Some results of this analysis are shown for two wavenumber regions in Figure 4. Given the line broadening evident in the primary spectra, the wavenumber values must be susceptible to large uncertainties, though the peak at ~580 cm^{-1} is better defined than the one at ~360 cm^{-1}. However, two features are common to both sets of data. There is a discontinuity at X_{Ca} ~ 0.38, corresponding to the composition at which the *I*4/*mcm* structure gives way to the intermediate structure. Secondly, the wavenumbers appear to vary continuously across the composition X_{Ca} ~ 0.58, which defines the change from intermediate to *Pnma* structures.

Changes in line width

From Figure 3 it is apparent that, with increasing Ca content, the line widths in the spectra increase, reach a maximum, and then decrease again. Even though there is no real possibil-

ity of using conventional peak fitting routines for extracting line width, variations of the effective line width can be determined by the autocorrelation method (Malcherek et al. 1995; Salje and Bismayer 1997; Boffa Ballaran et al. 1998; Atkinson et al. 1999; Salje et al. 2000). Following Press et al. (1992) the autocorrelation function is defined as:

$$\mathrm{Corr}(g,\omega') = \int_{-\infty}^{+\infty} g(\omega+\omega')g(\omega)d\omega \qquad (8)$$

Corr(g,ω) is thus the product of the spectrum itself, g(ω), and the same spectrum, g(ω + ω'), after applying a shift, ω'. The advantage of this method lies in the fact that a weighted average of all peaks contributing to the chosen region of the measured data is calculated, and this average is proportional to the widths of the individual peaks. Figure 5 shows the variation of this value with ω' for the frequency range 100–507 cm^{-1} of the primary spectra shown in Figure 3. These autocorrelation spectra immediately distinguish different phases in the system. The *Pm*3*m* phase is shown at the top. It is followed by the tetragonal *I*4/*mcm* phase and the intermediate and the orthorhombic *Pnma* phase of the Ca end-member. Changes in the spectra occur at the same compositions as the structural changes marked in Figure 1 for room temperature.

In order to extract quantitative information from the autocorrelation spectra, a gaussian function of the form

$$G = k_0 \exp\left[-\left(\frac{x-k_1}{k_2}\right)^2\right] \qquad (9)$$

was used to fit the central peak of the autocorrelation function over different ranges of ω'. The fit parameter k_2, which is proportional to the line width of the autocorrelation spectra, was subsequently plotted versus ω for each fit and the final value of the effective line width (Δcorr) was taken as the value of k_2 extrapolated to ω' = 0. The results of these procedures are given as the parameter $\Delta\mathrm{corr}_{100-507}$, which is plotted against composition in Figure 6. With increasing Sr content the effective line width Δcorr increases to a maximum at composition $X_{Sr} \approx 0.5$

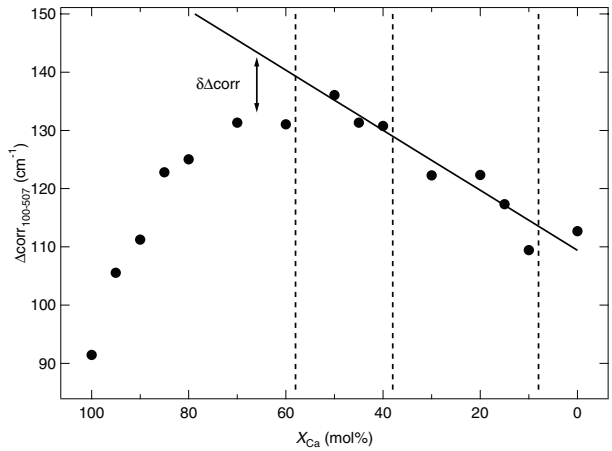

FIGURE 6. A possible interpretation of line width variations across the solid solution, as quantified by autocorrelation analysis of the 100–507 cm^{-1} spectral range. A straight line has been drawn through the data for samples with high Sr content to give a baseline. Deviations from this are defined as δΔcorr. In this interpretation, spectral line broadening increases with the addition of $CaTiO_3$ to $SrTiO_3$ until the composition $Ca_{0.6}Sr_{0.4}TiO_3$ is reached.

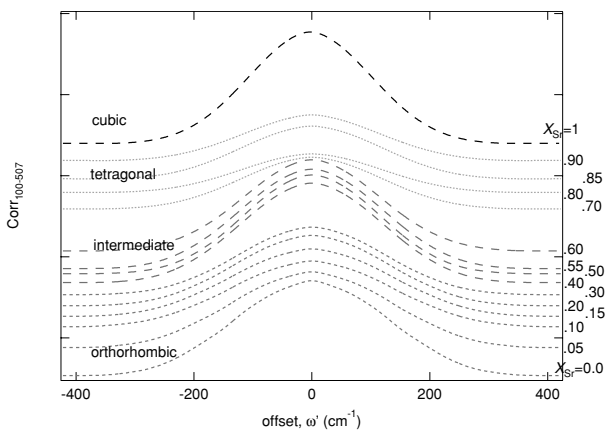

FIGURE 5. Autocorrelation spectra from a segment of spectra in the range 100–500 cm^{-1}. These clearly show a qualitative distinction between the different phases. The top spectrum belongs to the *Pm*3*m* phase. The following four spectra are from samples which have *I*4/*mcm* symmetry: they are much broader and do not reach the same maximum amplitude as the cubic end-member. The next three spectra are from the samples with compositions in the range of the intermediate stucture and are again quite distinct. The bottom five spectra are from samples in the *Pnma* stability field.

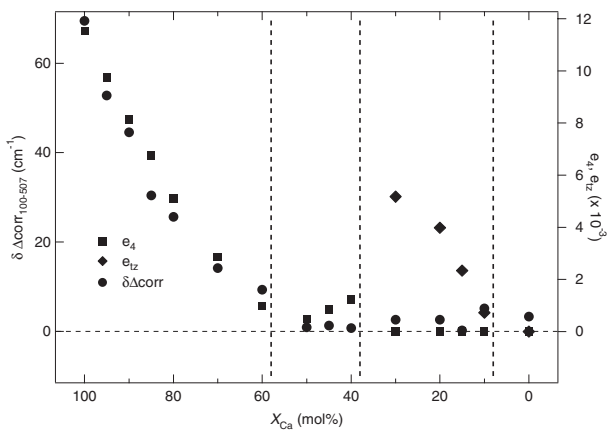

FIGURE 7. Comparison of δΔcorr from Figure 6 with spontaneous strains from Figure 2b. From the interpretation given in Figure 6, there is close correlation between spectral line broadening and the orthorhombic shear strain e_4, but none with the tetragonal shear strain e_{tz}.

and subsequently decreases. By analogy with the analysis of phase transitions in silicates, line widths are expected to decrease with increasing values of the order parameter for a phase transition (Bismayer 1990; Salje and Bismayer 1997; Salje et al. 2000). In the interpretation of the data implied by the straight line shown in Figure 6, cubic and tetragonal structures have been grouped together to represent a high symmetry state. The data do not by themselves permit discrimination between the two. Deviations from this line are expressed as an excess parameter, δΔcorr, which increases with increasing $CaTiO_3$ content. The spectral parameter δΔcorr is compared with the macroscopic strains in Figure 7. The systematic changes of δΔcorr are found to reflect the variation of the shear strain e_4, which describes the distortion of the orthorhombic phase as a result of the incorporation of Sr. Both e_4 and δΔcorr tend to zero at $X_{Ca} \approx 0.58$, the composition at which the *Pnma* structure gives way to the intermediate structure. In this interpretation, δΔcorr seems not to reflect the tetragonal shear e_{tz}, though data for the cubic range are limited.

Removing the background

A third way to extract information about the transformation behavior is to determine intensity variations of absorption peaks occurring exclusively in spectra from the low symmetry structures. Common to all spectra across the solid solution are the extremely broad features centered around 330 and 580 cm^{-1}. Relatively sharp peaks in the orthorhombic spectra are superimposed on these. The spectrum for crystals with composition $X_{Sr} = 0.9$ was used as a crude estimate of a non-linear baseline. This was subtracted from the other spectra in the spectral range 100–500 cm^{-1}, and the total remaining intensity (I–$I_{0.9}$) is shown as a function of composition in Figure 8. The resulting variations show a pattern which is broadly similar to that shown by the variations of δΔcorr and the frequency of the broad band at ~580 cm^{-1}.

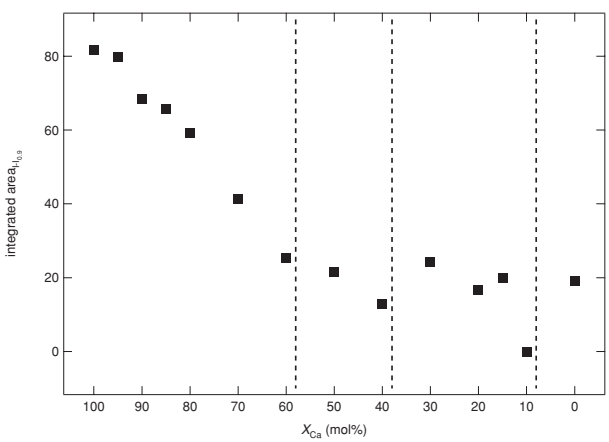

FIGURE 8. Changes in integrated intensity of the relatively sharp peaks in the spectra across the solid solution using the spectrum for $Ca_{0.1}Sr_{0.9}TiO_3$ as a reference to subtract the two underlying broad peaks. A change in trend is again apparent at the composition representing the change of structure from intermediate to *Pnma*.

DISCUSSION

In spite of the difficulty in dealing with the typically broadened absorption IR spectra of perovskites, it has been possible to extract quantitative information relating to frequency, intensity, and line broadening from spectra obtained from the $CaTiO_3$-$SrTiO_3$ solid solution. Data for ω_{576} (Fig. 4), $\Delta corr_{100–507}$ (Fig. 6) and I-$I_{0.9}$ (Fig. 8) all define essentially the same trends. From the macroscopic shear strain e_{tz}, it is apparent that the $Pm3m \leftrightarrow I4/mcm$ transition is continuous as a function of composition at room temperature. The resolution of the spectroscopic data is not good enough to conclude that the transition is also continuous on a local length scale, but the ω_{576} and $\Delta corr_{100–507}$ data are at least consistent with this possibility. The $I4/mcm \leftrightarrow$ orthorhombic transition at $X_{Ca} = 0.58$ is certainly discontinuous with respect to the evolution of shear strain (Fig. 2b), and the data for ω_{576} and I-$I_{0.9}$ are probably also consistent with the shear strain. The main effects seen in the spectroscopic data, however, relate to the development of the *Pnma* structure for $CaTiO_3$ rich compositions. Each of the spectroscopic parameters follow essentially the same trend as shown by the orthorhombic shear strain e_4. This distortion of the perovskite structure thus seems to dominate the structural evolution at both the microscopic and macroscopic length scales.

Howard et al. (2001) and Ranjan et al. (2001) have shown by electron diffraction from thin crystals that samples with intermediate compositions have space group *Pnma*, and not *Cmcm* as suggested by Ball et al. (1998). From the autocorrelation spectra in Figure 5, however, it is apparent that crystals with compositions in the range $X_{Sr} \approx 0.4$ to ≈ 0.6 differ systematically from crystals with $X_{Sr} < 0.4$. These intermediate crystals also have close to zero orthorhombic shear strain. Thus, although the symmetry of the crystals may be *Pnma*, any distortions from cubic geometry remain small, both at the macroscopic length scale and at a phonon length scale. The cause of these unusual properties requires further investigation, but one possible origin could be frustration effects. As $SrTiO_3$ content increases across the solid solution, the energy difference between the *Pnma* and *I*4/*mcm* diminishes. Any local tendency to develop a *Pnma* distortion could then be opposed by almost equal and opposite tendencies to develop *I*4/*mcm* distortions. There must also be local strain effects of having almost equal proportions of A site cations with different sizes, which would further hinder correlated distortions of the perovskite structure. The "intermediate" structure would thus be one in which some correlation of structural distortions occurs to reduce the symmetry to *Pnma* but in which the magnitude of these correlated distortions is constrained to be very small.

In this context it is worth pointing out that the maximum values of $\Delta corr_{100–507}$ occur at these intermediate compositions. This maximum in line broadening can be understood as representing a maximum in the local structural heterogeneity in $CaTiO_3$-$SrTiO_3$ perovskites. Correlated distortions of larger magnitude then develop from the frustrated structure as the proportion of Ca to Sr increases. There is no evidence in the strain or spectroscopic data that this development is anything other than continuous in character.

ACKNOWLEDGMENTS

The authors thank M. Zhang for help with the IR experiments, E.K.H. Salje for helpful discussions and two anonymous reviewers for helpful comments. This work was performed within and was financially supported by the European Union TMR-Network on Mineral Transformations (contract no. ERB-FMRX-CT-97-0108).

REFERENCES CITED

Atkinson, A.J., Carpenter, M.A., and Salje, E.K.H (1999) Hard mode infrared spectroscopy of plagioclase feldspars. European Journal of Mineralogy, 11, 7–21.

Ball, C.J., Begg, B.D., Cookson, D.J., Thorogood, G.J., and Vance, E.R. (1998) Structures in the system $CaTiO_3/SrTiO_3$. Journal of Solid State Chemistry, 139, 238–247.

Bismayer, U. (1990) Hard mode Raman spectroscopy and its applications to ferroelastic and ferroelectric phase transitions. Phase Transitions, 27, 211–267.

Boffa Ballaran, T., Carpenter, M.A., Domeneghetti, M.C., Salje, E.K.H., and Tazzoli, V. (1998) Structural mechanisms of solid solution and cation ordering in augite-jadeite pyroxenes: II. A microscopic perspective. American Mineralogist, 83, 434–443.

Carpenter, M.A., Becerro, A.I., and Seifert, F. (2001) Strain analysis of phase transitions in $(Ca,Sr)TiO_3$ perovskites. American Mineralogist, 86, 348–363.

Ceh, M., Kolar, D., and Golic, L. (1987) The Phase diagram of $CaTiO_3$-$SrTiO_3$. Journal of Solid State Chemistry, 68, 68–72.

Dec, J. and Kleemann, W. (1998) From Barrett to Generalized Quantum Curie-Weiss Law. Solid State Communications, 106, 695–699.

Fleury, P.A. and Worlock, J.M. (1968) Electric field induced Raman scattering in $SrTiO_3$ and $KTaO_3$. Physical Review, 174, 613–623.

Hirata, T., Ishioka, K., and Kitajima, M. (1996) Vibrational spectroscopy and X-ray diffraction of perovskite compounds $Sr_{1-x}M_xTiO_3$ (M=Ca, Mg; $0 \le x \le 1$). Journal of Solid State Chemistry, 124, 353–359.

Howard, C.J., Withers, R.L., and Kennedy, B.J. (2001) Space group and structure for the perovskite $Ca_{0.5}Sr_{0.5}TiO_3$. Journal of Solid State Chemistry, 160, 8–12.

Kleemann, W., Dec, J., and Westwanski, B. (1998) Susceptibility scaling behaviour of quantum paraelectric $SrTiO_3$:Ca. Physical Review B, 58, 8985–8990.

Lemanov, V.V. (1997) Phase transitions in $SrTiO_3$-based solid solutions. Physics of the Solid State, 39, 1468–1473.

Lu, R. and Hofmeister, A.M. (1994) Infrared spectroscopy of $CaGeO_3$ Perovskite to 24 Gpa and Thermodynamic Implications. Physics and Chemistry of Minerals, 21, 78–84.

Malcherek, T., Kroll, H., Schleiter, M., and Salje, E.K.H. (1995) The kinetics of the monoclinic to monoclinic phase transition in $BaAl_2Ge_2O_8$-feldspar. Phase Transitions, 55, 199–215.

Mitsui, T. and Westphal, W.B. (1961) Dielectric and X-ray studies of $Ca_xBa_{1-x}TiO_3$ and $Ca_xSr_{1-x}TiO_3$. Physical Review, 124, 1354–1359.

Press, W. H., Teukolsky, S. A., Vetterling, W. T., and Flannery, B. P. (1992) Numerical recipes in FORTRAN, 492 p. Cambridge University Press, Cambridge, U.K.

Qin, S., Becerro, A.I., Seifert, F., Gottsmann, J., and Jiang, J. (2000) Phase transitions in $Ca_{1-x}Sr_xTiO_3$ perovskites: effects of composition and temperature. Journal of Materials Chemistry, 10, 1–8.

Ranjan, R. and Pandey, D. (2001) Antiferroelectric phase transition in $(Sr_{1-x}Ca_x)TiO_3$ ($0.12 \le x \le 0.40$): I. Dielectric studies. Journal of Physics: Condensed Matter, 13, 4239–4249.

Ranjan, R., Pandey, D., Schuddinck, W., Richard, O., De Meulenaere, P., Van Landuyt, J., and Van Tendeloo, G. (2001) Evolution of crystallographic phases in $(Sr_{1-x}Ca_x)TiO_3$ with composition (x). Journal of Solid State Chemistry, 162, 20–28.

Ringwood, A.E. (1985) Disposal of high-level nuclear wastes; a geological perspective. Mineralogical Magazine, 49, 159–176

Salje, E.K.H. and Bismayer, U. (1997) Hard mode spectroscopy: The concept and applications. Phase Transitions, 63, 1–75.

Salje, E.K.H., Carpenter, M.A., Malcherek, T., and Boffa Ballaran, T. (2000) Autocorrelation analysis of infrared spectra from minerals. European Journal of Mineralogy, 12, 503–519.

MANUSCRIPT RECEIVED OCTOBER 29, 2001
MANUSCRIPT ACCEPTED MAY 2, 2002
MANUSCRIPT HANDLED BY SIMON C. KOHN